AWARD NUMBER: W81XWH-19-1-0616

TITLE: Ultrahigh Field MRI Detection of Biomarkers in Post Traumatic Epilepsy

PRINCIPAL INVESTIGATOR: Rebecca Feldman

CONTRACTING ORGANIZATION: Mount Sinai Hospital
Hess Center for Science and Medicine
New York, NY, 10029

REPORT DATE: September 2020

TYPE OF REPORT: Annual Report

PREPARED FOR: U.S. Army Medical Research and Development Command
Fort Detrick, Maryland 21702-5012

REPORT DOCUMENTATION PAGE

Form Approved
OMB No. 0704-0188

1. REPORT DATE	2. REPORT TYPE	3. DATES COVERED
September 2020	Annual	30Aug2019-29Aug2020

4. TITLE AND SUBTITLE

Ultrahigh Field MRI Detection of Biomarkers in Post Traumatic Epilepsy

5a. CONTRACT NUMBER

5b. GRANT NUMBER
W81XWH-19-1-0616

5c. PROGRAM ELEMENT NUMBER

6. AUTHOR(S)
Rebecca Feldman
Rebecca.feldman2@mountsinai.org

E-Mail:

5d. PROJECT NUMBER

5e. TASK NUMBER

5f. WORK UNIT NUMBER

7. PERFORMING ORGANIZATION NAME(S) AND ADDRESS(ES)

Mount Sinai Hospital, Hess Center for Science and Medicine, 1470 Madison Ave, New York, NY, 10029

8. PERFORMING ORGANIZATION REPORT NUMBER

9. SPONSORING / MONITORING AGENCY NAME(S) AND ADDRESS(ES)

U.S. Army Medical Research and Development Command
Fort Detrick, Maryland 21702-5012

10. SPONSOR/MONITOR'S ACRONYM(S)

11. SPONSOR/MONITOR'S REPORT NUMBER(S)

12. DISTRIBUTION / AVAILABILITY STATEMENT

Approved for Public Release; Distribution Unlimited

13. SUPPLEMENTARY NOTES

14. ABSTRACT

Post traumatic epilepsy (PTE) can be characterized as recurring seizures which develop after traumatic brain injury. There is often a significant delay between the manifestation of seizures and the initial injury. There is increasing evidence that suggests that epilepsy is a disease involving a network of abnormalities, and ultra-high field magnetic resonance imaging (MRI), such as systems operating at fields strengths of 7 Tesla (7T), enable exceptionally high-contrast, high-resolution *in vivo* imaging of the brain. If we can detect imaging biomarkers of changes specific to epileptogenesis following TBI we may be able to eventually develop treatments which target those mechanisms for antiepileptogenic therapy without compromising recovery from TBI or worsening the effects of other TBI co-morbidities.

We are recruiting patients with TBI, PTE, and healthy controls as part of an imaging study. Patients with TBI are matched with the recruited PTE patients and healthy controls. Volunteer image data will be collected using an optimized TBI imaging protocol. The data will be processed to explore suspected biomarkers of epilepsy in all volunteers.

15. SUBJECT TERMS
Post Traumatic Epilepsy, Traumatic Brain Injury, Ultra High Field MRI, 7T MRI

16. SECURITY CLASSIFICATION OF:			17. LIMITATION OF ABSTRACT	18. NUMBER OF PAGES	19a. NAME OF RESPONSIBLE PERSON
					USAMRMC
a. REPORT	b. ABSTRACT	c. THIS PAGE		31	19b. TELEPHONE NUMBER *(include area code)*
Unclassified	Unclassified	Unclassified	Unclassified		

Standard Form 298 (Rev. 8-98)
Prescribed by ANSI Std. Z39.18

TABLE OF CONTENTS

1. INTRODUCTION:

Post traumatic epilepsy (PTE) can be characterized as recurring seizures develop after traumatic brain injury. There is often a significant delay between the manifestation of seizures and the initial injury. There is increasing evidence that suggests that epilepsy is a disease involving a network of abnormalities. 7 Tesla MRI, enables exceptionally high-contrast, high-resolution *in vivo* imaging of the brain. We are recruiting patients with TBI, PTE, and healthy controls as part of an imaging study. The data will be processed to explore suspected biomarkers of epilepsy in all volunteers.

2. KEYWORDS:

Post Traumatic Epilepsy, Traumatic Brain Injury, Ultra High Field MRI, 7T MRI

3. ACCOMPLISHMENTS:

What were the major goals of the project?

Specific Aim 1 - Specific Aim 1 – Leverage new 7T structural, spectroscopic, and diffusion MRI tools to identify network changes in the brain associated with PTE (Months 1-20)
Milestone 2: Protocol Optimized with finalized Data Collection Instruments - December 2019 (100%)
Milestone 3: Complete enrollment and data acquisition of subjects, PTE and HC – April 2021 (6%)
Milestone 4: Define biomarkers of PTE – April 2021 (0%)
Specific Aim 2 – Identify biomarkers which can be used to differentiate PTE from non-epileptogenic TBI (Months 4-24)
Milestone 5: Complete enrollment and data acquisition of TBI subjects – May 2021 (0%)
Milestone 6: Quantification of metrics related to PTE and TBI – August 2021 (0%)

What was accomplished under these goals?

1) Major Activities
Major activities this year have focused around establishing the research program, obtaining institutional permissions to conduct research, communicating and collaborating with the co-investigators. We hired staff to carry out elements of the research and developed, tested, and optimized the protocol as well as developing and testing image processing capabilities

We applied for and received permission to resume research at Mount Sinai after the shutdown due to COVID-19. PTE patients have been contacted, and screened for participation.

1) Major Activities Cont.

Milestone 1: IRB Approval
Protocol Approvals: Both IRB and HRPO approval was obtained.
Permission to resume human research was acquired following the shutdown due to COVID-19

Milestone 2: Protocol Optimization
Personnel: A clinical coordinator was hired and has been trained on the protocol

Data Acquisition and Image Analysis: A Redcap database has been established, and populated with forms. The final set of data collection instruments were agreed upon based on preliminary data collected in the Fall. An IRB amendment was submitted and approved.

Milestone 3: Recruitment: Continuing IRB approval was also obtained. Following the resumption of research at Mount Sinai, PTE patients have been contacted, and screened for participation. Recruitment details, following a CONSORT chart type of information is included in Appendix 1

Milestone 4: Define biomarkers of PTE
Image analysis pipelines were developed to facilitate network analysis of PTE. Tool was prototyped on pilot data set.

A report on the image analysis tools developed for this project was accepted for publication

What opportunities for training and professional development has the project provided?

Undergraduate Research Trainees: Two fourth year honors students have joined my research lab for their thesis. Their projects center around developing and optimizing image processing tools for the data to be acquired this year.

These students attended the ISMRM Virtual Meeting in August, and participated in the weekend educational courses.

How were the results disseminated to communities of interest?

Nothing to Report

What do you plan to do during the next reporting period to accomplish the goals?

We plan to complete recruitment and scanning over the next 6-9 months, upload all acquired data sets to FITBIR, and process the data, identifying biomarkers of epilepsy.

PTE Enrollment: Presented at the Monthly Mount Sinai Epilepsy meeting in October in order to accelerate recruitment. We plan to collaborate with additional epileptologists in the Mount Sinai Health System to expand the recruitment pool. Epileptologist will screen for Traumatic Brain Injury within their own clinics and refer them to our study. Additionally, we've distributed IRB approved passive recruitment materials to several epilepsy support groups. This effort to expand enrollment to meet our recruitment goals should not have an impact on the budget.

TBI Enrollment: Presented at the Brain Injury Association of New York State (BIANYS) New York City Chapter meeting. Traumatic Brain Injury (TBI) patients attended the conference call and were able to sign up for participation.

4. IMPACT:

What was the impact on the development of the principal discipline(s) of the project?

Technical development: we have developed a technique to detect and measure the venous vascular network in the brain using 7T MRI. This technique lets us visualize and quantify the vessels through which blood drains out of the brain. This additional metric may help us understand what parts of the brain are affected after injury and track the progression of the disease.

The Project Narrative described a proof of concept analysis of blood vessel structure through automatic segmentation of susceptibility-weighted imaging data. Changes to vasculature is thought to be indicative of epileptic pathology. Analysis of blood vessels in patients with PTE, healthy controls, and TBI patients may help identify changes with in the brain that lead to the onset of epilepsy.

What was the impact on other disciplines?

The metric designed to measure and quantify venous vasculature is also of interest to neurologists studying multiple sclerosis. This processing tool is being used to aide in the evaluation of perivascular spaces around a central vein. This metric is being used to investigate response to treatment in relapsing remitting multiple sclerosis.

What was the impact on technology transfer?

Nothing to Report

What was the impact on society beyond science and technology?

Nothing to Report

5. CHANGES/PROBLEMS:

Changes in approach and reasons for change

Nothing to Reports

Actual or anticipated problems or delays and actions or plans to resolve them

Recruitment Delay: The worldwide pandemic has resulted in a significant recruitment delay due to uncertainty of the pandemic in NYC participants are hesitant to come in for in-person research at this time. To accelerate PTE subject recruitment, we are expanding the pool of recruiting physicians, and focusing on recruitment and screening. We are also currently working with Mount Sinai Hospital's social media team to promote the study on their website and other social media outlets.

We anticipate that we will require additional time to complete recruitment. This will delay the final analysis and data reporting. Once we have assessed our recruitment rate, we plan to apply for a no-cost extension in order to ensure that the analysis can be completed.

Changes that had a significant impact on expenditures

Due to the delay in recruitment, subject reimbursement has not yet been made for the expected number of participants. Similarly, there have not yet been charges for the expected use of the MRI scanner. We expect that these charges will be made over the next year as we accelerate recruitment to meet recruitment targets.

Significant changes in use or care of human subjects, vertebrate animals, biohazards, and/or select agents

Decreased one-on-one contact during intake and screening: All screening which can be done over the phone is now required to be done over the phone. This includes the initial safety screening, consent process, and questionnaires. This was done to decrease-in person contact in response to the on-going COVID-19 pandemic.

Imaging Facility Cleaning Protocol Changes: The imaging facility initiated a number of changes related to ensuring volunteer safety and reduce/eliminate virus transmission. This includes the use of face masks in public areas and enhanced cleaning protocols.
The program for the protection of human subjects approved our research resumption

SUBMITTED TO AND APPROVED BY:

- Mount Sinai IRB: Submission 19-01970
- Mount Sinai IRB: HSM: 19-00542 - Approval 06/25/2019; Expires (renewal required by) 06/16/2020
- HRPO: Log Number E00857.1a (Approval Memorandum: 10/31/2019)
- Mount Sinai IRB: Amendment Approved 03/30/2020
- Mount Sinai IRB: Continuation – Approved 06/16/2020

Significant changes in use or care of vertebrate animals

Nothing to Report

Significant changes in use of biohazards and/or select agents

Nothing to Report

6. PRODUCTS:

- **Publications, conference papers, and presentations**

Journal publications.

Feldman RE, Marcuse LV, Verma G, Brown SSG, Rus A, Rutland JW, Delman BN, Balchandani P, Fields MC. "Seven-tesla susceptibility-weighted analysis of hippocampal venous structures: Application to magnetic-resonance-normal focal epilepsy." Epilepsia. 2020. doi: 10.1111/epi.16433. Epub 2020 Feb 4. Acknowledgement of federal support (yes)

The above manuscript reports on images acquired in MTLE patients. The major revision of the data analysis for this manuscript occurred over the late fall. At the same time, we were focussing our efforts on developing the data analysis tools required to analyze the images we intend to obtain under this award. The SWI imaging protocol used on the MTLE patients was substantively similar to the planned PTE imaging protocol, thus we were able to reprocess the previously acquired MTLE images through the data analysis tool that we refined during Q4 of 2019.

We received permission to delay the submission of the revisied manuscript until January 1, 2020 so we could take advantage of the reduction in false positives provided by the newly developed data analysis software. The above listed publication describes the methods we developed for the purposes of analyzing the vessels in the PTE data set once acquired.

Books or other non-periodical, one-time publications.

Nothing to Report

Other publications, conference papers and presentations.

Conference Presentation:
Brown S, Dams-O'Connor K, Balchandani P, **Feldman RE**. "An MRI traumatic brain injury case study at 7Tesla: pre- and post- injury structural network and volumetric reorganization and recovery", *Proceedings of the ISMRM 28th Scientific Meeting, Virtual*, #2011 (August 2020) Acknowledgement of Federal Support (yes – in poster)

- **Website(s) or other Internet site(s)**

Nothing to Report

- **Technologies or techniques**

As described in the published manuscript, we have developed a technique to detect and measure the venous vascular network in the brain using susceptibility weighted imaging at 7T MRI. This technique lets us visualize and quantify the vessels through which blood drains out of the brain. This additional metric may help us understand what parts of the brain are affected after injury and track the progression or development of epilepsy.

Vascular structure may play a significant role in epileptic pathology, and a robust *in vivo* method of assessing this would facilitate the investigation of changes to vasculature associated with TBI and PTE in relation to healthy controls. This data analysis was performed on data acquired using a 7-T MRI scanner, and was optimized for SWI images acquired using the following sequence parameters (TA = 7:30, voxel size 0.2x0.2x1.5 mm^3, TR = 23 milliseconds, TE = 14 milliseconds, FA = 12°, matrix = 1024x832, BW = 150 Hz/pixel, image acceleration factor [iPAT] = 3). The technique makes use of structural images acquired using a T1-weighted sequence (Figure 1A).

Minimum intensity projection images through five (5) contiguous slices were produced from the magnitude of the SWI acquisition (Figure 1 B). Segmentation of the T1-weighted image were used to isolate the region of interest in the brain, and the SWI and T1-weighted images were co-registered (Figure 1C). A modified Frangi filter, implemented in MATLAB was used to detect potential venous structures, and the principle direction was found by finding the eigen values of the Hessian matrix.

To identify vessels, the objects detected were linked using nearest-neighbors (across all 3 dimensions), and networks shorter than 4 voxels were excluded.

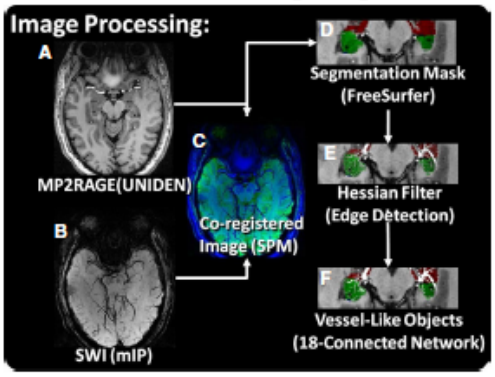

Figure 1: Image Processing Flow Chart

The protocol was validated against manually traced vessels across 13 non-contiguous axial mIP slices of a control SWI image representing the brain from the basal ganglia to the vertex. For comparison, the vessel tracing protocol was applied to the same slices. The manual and automatic vessel tracings were compared and, sensitivity and positive predictive value were calculated. The validation set contained a total 1245 manually traced vessels, and 1444 veins were identified by the automated method. A total of 1215 veins were concordant between the two methods. A total of 229 objects were labeled as veins by the automated method where none was indicated in the manual tracing. A total of 30 veins were seen only by the manual tracing. The sensitivity of the automated tracing technique is show in Figure 2 along with summary statistics. The sensitivity ranged between 0.81 and 1.0. The positive predictive value of the method ranged between 0.63 and 1.00.

The false positives identified by comparison between the manual and automatic tracings were re-examined. 43 out of the 46 objects identified by the automated tool but not the manual tracing were re-classified after re-examination.

Although the majority of the structures identified by the automatic segmentation were visible to both the automatic and manual segmentation, each protocol uniquely identified a set of vessel structures. The assessment showed that manual segmentation was more accurate in regions near the sinuses or where low overall signal rendered the SWI less reliable. However, the automatic segmentation technique was more rapid and did not suffer from inconsistencies due to manual rater fatigue and was better able to assess information across multiple imaging planes to identify vessels traveling perpendicular to the plane of analysis.

This technique was published in Epilepsia in 2020.

A

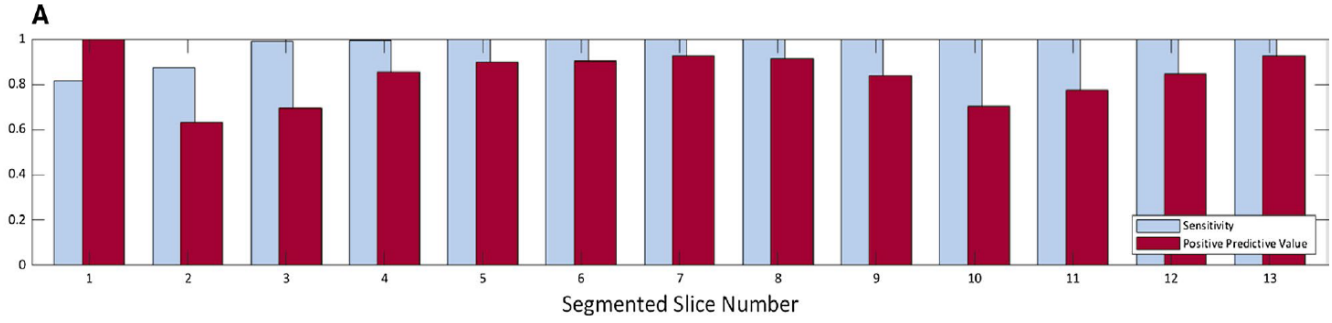

B

	# True Positive	# False Positive	# False Negative	Sensitivity	Positive Predictive Value
Overall	1215	229	30	0.98	0.84

Figure 2: Comparison of Automated and manual segmentation

Inventions, patent applications, and/or licenses

Nothing to Report

- **Other Products**

Nothing to Report

7. PARTICIPANTS & OTHER COLLABORATING ORGANIZATIONS

What individuals have worked on the project?

Name: Rebecca Feldman
Project Role: Project Director
Researcher Identifier: 0000-0001-8403-9807
Nearest person month worked: 4
Contribution to Project: Dr. Feldman has developed research protocol and coordinated with the IRB to modify the protocol. She is also coordinating the data collection and development of analysis tools.

Name: Alara Akyatan
Project Role: Clinical Research Coordinator
Nearest person month worked: 4
Contribution to Project: Alara was re-deployed by Mount Sinai during April and May. She has coordinated PTE patient identification and recruitment. She has also identified and recruited non-PTE TBI participants.

Name: Stephanie Brown
Project Role: Postdoctoral Fellow (data analysis)
Nearest person month worked: 1
Contribution to Project: Stephanie analyzed diffusion data to evaluate network changes following TBI.

Name: Seger Nelson
Project Role: Undergraduate Research Assistant
Nearest Person Month worked: 2
Contribution to Project: Post-processing pipeline and data analysis

Name: Priti Balchandani
Project Role: Co-investigator/Collaborator
Nearest person month worked: 1
Contribution to Project: Dr. Balchandani advised on and facilitated the development of the imaging protocol and the resumption of research.

Name: Kristen Dams O'Connor
Project Role: Co-investigator/Collaborator
Nearest person month worked: 1
Contribution to project: Dr. Dams O'Connor advised and guided the development of the neurological testing protocol, and lent her expertise to the training of the clinical coordinator

Has there been a change in the active other support of the PD/PI(s) or senior/key personnel since the last reporting period?

New Funding
Image acquisition and analysis tools for magnetic resonance imaging near brain injury
NSERC Discovery Grant RGPIN-2020-06005
April 2020 – March 2025
CAD /y

What other organizations were involved as partners?

University of British Columbia
Location of Organization: Kelowna, British Columbia, Canada
Partners contribution to the project: Office space for research and data analysis and undergraduate trainee.

8. SPECIAL REPORTING REQUIREMENTS

COLLABORATIVE AWARDS:

QUAD CHARTS:

Ultrahigh Field MRI Detection of Biomarkers in Post Traumatic Epilepsy

Log Number: EP180006

Award Number: W81XWH-19-1-0616

PI: Rebecca Feldman **Org:** Mount Sinai **Award Amount: $508,490**

Study/Product Aim(s)

- Leverage new 7T structural, spectroscopic, and diffusion MRI tools to identify network changes in the brain associated with Post Traumatic Epilepsy
- Identify biomarkers which can be used to differentiate PTE from TBI

Approach

We hypothesize in cases of PTE, epileptogenic changes occur in the beyond the site of initial injury. We believe that through the analysis of 7T MRI data we will be able to detect reorganization in neuronal circuitry, metabolic function, and structural changes which lead to the development of PTE following TBI.

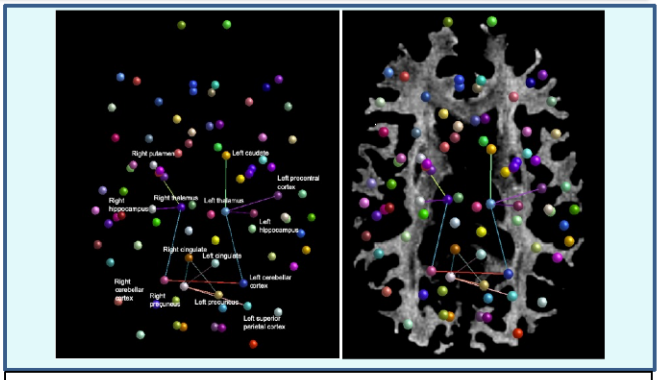

We segmented hippocampus subnuclei and the amygdala and analyzed the structural connectomes for the subjects.

Timeline and Cost

Activities CY	19	20	21	
Enroll and acquire data from patients with PTE				
Identify imaging biomarkers of PTE				
Enroll and acquire data from patients with TBI				
Differentiate biomarkers of PTE and TBI				
Estimated Budget ($508 K)	**$63K**	**$255K**	**$191**	

Updated: Mount Sinai Aug 31, 2020

Goals/Milestones (Example)

CY19 Goal – Establish experimental protocol

☑ Develop experimental protocol

☑ Acquire approval

☑ Optimize imaging protocol

☑ **CY20 Goals** – Subject enrollment and data acquisition

☑ Validate Imaging protocol

☐ Enroll subjects and acquire data

☐ Finalize image analysis techniques

CY21 Goal – Continued data acquisition and image analysis

☐ Complete subject enrollment and data acquisition

9. APPENDICES

Appendix 1: Recruitment Details

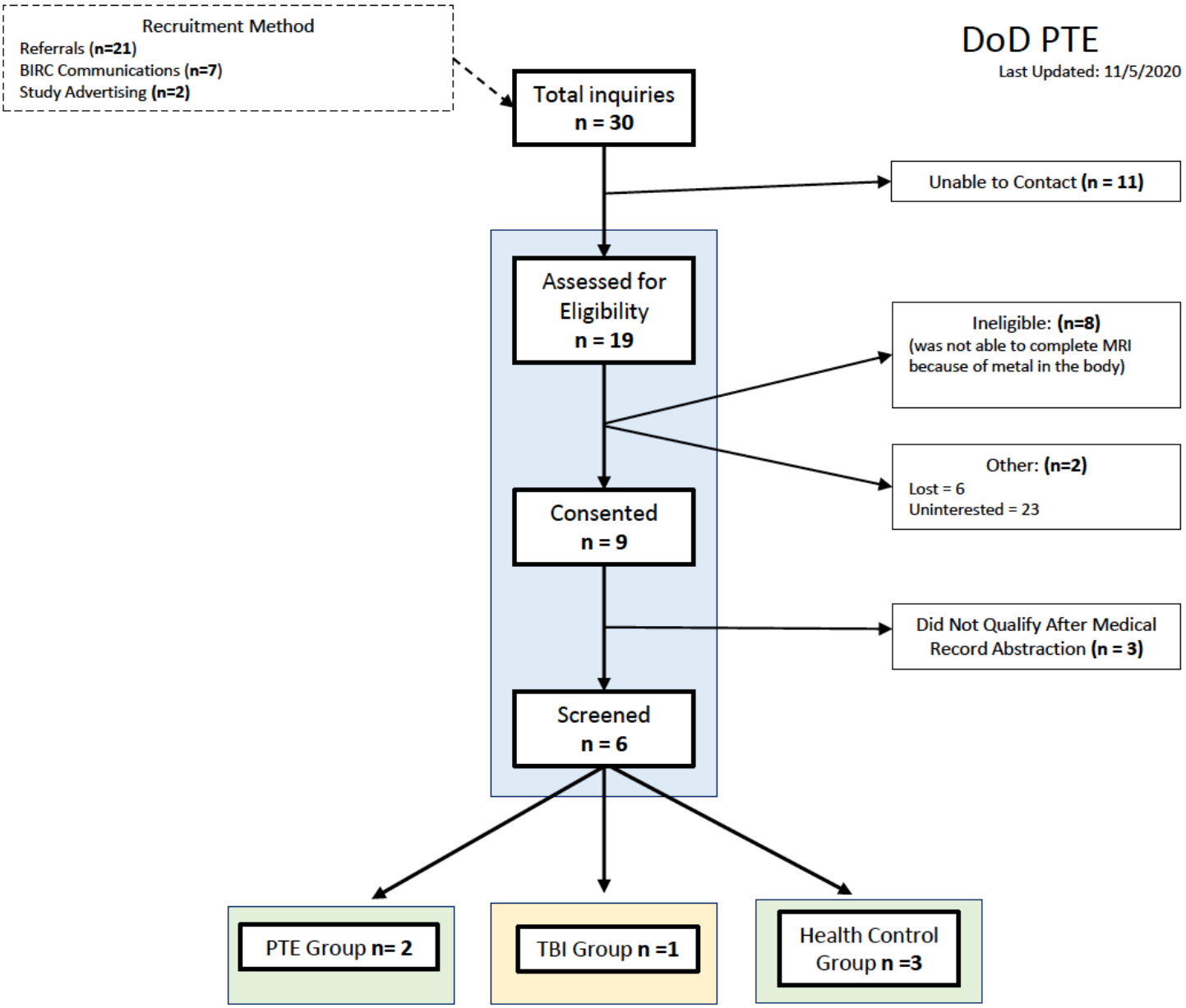

Appendix 2: 7T SWI of hippocampal venous structures cover page

Received: 1 August 2019 | Revised: 1 January 2020 | Accepted: 1 January 2020
DOI: 10.1111/epi.16433

FULL-LENGTH ORIGINAL RESEARCH

Epilepsia

Seven-tesla susceptibility-weighted analysis of hippocampal venous structures: Application to magnetic-resonance–normal focal epilepsy

Rebecca Emily Feldman[1,2,3] | **Lara Vanessa Marcuse**[4] | **Gaurav Verma**[2,3] | **Stephanie Sian Gabriella Brown**[5] | **Alexandru Rus**[2] | **John Watson Rutland**[2] | **Bradley Neil Delman**[2,3] | **Priti Balchandani**[2,3] | **Madeline Cara Fields**[4]

[1]Department of Computer Science, Math, Physics, and Statistics, University of British Columbia, Kelowna, British Columbia, Canada

[2]Translational and Molecular Imaging Institute, Icahn School of Medicine at Mount Sinai, New York, New York

[3]Department of Radiology, Icahn School of Medicine at Mount Sinai, New York, New York

[4]Department of Neurology, Mount Sinai Hospital, New York, New York

[5]Department of Psychiatry, University of Cambridge, Cambridge, UK

Correspondence
Rebecca Emily Feldman, Department of Computer Science, Math, Physics, and Statistics, University of British Columbia, Kelowna, BC, Canada.
Email: rebecca.feldman@ubc.ca

Funding information
National Institute of Neurological Disorders and Stroke, Grant/Award Number: R00 NS070821; U.S. Department of Defense, Grant/Award Number: DOD W81XWH-18-ERP-IDA; National Institute of Mental Health, Grant/Award Number: NIH R01 MH109544

Abstract

Objective: Vascular structures may play a significant role in epileptic pathology. Although previous attempts to characterize vasculature relative to epileptogenic zones and hippocampal sclerosis have been inconsistent, an in vivo method of analysis would assist in resolving these inconsistencies and facilitate a comparison against healthy controls in a human model. Magnetic resonance imaging is a noninvasive technique that provides excellent soft tissue contrast, and the relatively recent development of susceptibility-weighted imaging has dramatically improved the visibility of small veins.

Methods: We built and tested a Hessian-based segmentation technique, which takes advantage of the increased signal and contrast available at 7 T to detect venous structures in vivo. We investigate the ability of this technique to quantify vessels in the brain and apply it to an asymmetry analysis of vessel density in the hippocampus in patients with mesial temporal lobe epilepsy (MTLE) and neocortical epilepsy.

Results: Vessel density was highly symmetric in the hippocampus in controls (mean asymmetry = 0.080 ± 0.076, median = 0.05027), whereas average vessel density asymmetry was greater in neocortical (mean asymmetry = 0.23 ± 0.17, median = 0.14) and MTLE (mean asymmetry = 0.37 ± 0.46, median = 0.26) patients, with the decrease in vessel density ipsilateral to the suspected seizure onset zone. Post hoc testing with one-way analysis of variance and Tukey post hoc test indicated significant differences in the group means ($P < .02$) between MTLE and the control group only.

Significance: Asymmetry in vessel density in the hippocampus is visible in patients with MTLE, even when qualitative and quantitative measures of hippocampal asymmetry show little volumetric difference between epilepsy patients and healthy controls.

KEYWORDS
7-T MRI, hippocampus, nonlesional focal epilepsy, SWI, temporal lobe epilepsy

Priti Balchandani and Madeline Cara Fields are senior authors.

1 | INTRODUCTION

Epilepsy is a chronic condition that is characterized by recurrent seizures and actively affects approximately 1%-8% of the worldwide population.[1–5] Mesial temporal lobe epilepsy (MTLE) is the most common seizure type in adult epilepsy. MTLE is often drug-resistant and difficult to clinically manage. One of the most frequent magnetic resonance imaging (MRI) findings in adult MTLE is hippocampal sclerosis, which is characterized by gliosis and neuronal loss.[6–9]

In vivo identification of hippocampal volume (HV) asymmetry and of a hyperintense lesion on structural MRI scans are both key indicators of hippocampal sclerosis. However, even patients without a clear lesion or volume asymmetry on presurgical imaging who undergo successful surgery (guided by seizure semiology and both scalp and intracranial electroencephalography [EEG]) can have distinct, epileptogenic abnormalities identified in the resection via postsurgical histopathology.[10,11] This suggests that there are discrete structural abnormalities that are not well characterized by current imaging protocols and analysis.

Vascular structures may play a significant role in epileptic pathology. In analysis of sclerotic hippocampi of temporal lobe epilepsy patients, changes in permeability of the blood-brain barrier have been reported.[12–14] Although previous attempts to characterize vasculature relative to epileptogenic zones and hippocampal sclerosis have been inconsistent, an increase in hippocampal vasculature, found through examination of immunohistochemistry markers such as collagen IV and macroscopic observations of the epileptogenic zone, has been interpreted as evidence of an increase in hippocampal vasculature in MTLE.[15–22] However, this pattern is discordant with histochemical labeling studies employing alkaline phosphatase, a marker of endothelial cells in the blood-brain barrier, and both high-magnification light and electron microscopy, which suggest a decrease of blood vessels and visual identification of atrophic blood vessels in sclerotic hippocampi.[23–26] Existing techniques investigating alterations in vasculature during epilepsy have relied on ex vivo assessment of the resected hippocampus. An in vivo method would assist in resolving these inconsistencies and facilitate a comparison against healthy controls in a human model.

MRI is a noninvasive technique that provides excellent soft tissue contrast, and the relatively recent development of susceptibility-weighted imaging (SWI) has dramatically improved the visibility of small veins.[27–29] A number of algorithms making use of Hessian filters have been proposed to facilitate the segmentation of blood vessels made visible by SWI.[15,30–33] In this work, we build on the Steger algorithm[33] to create a Hessian-based segmentation technique, which takes advantage of the increased signal and contrast available at MRI strengths of 7 T to detect venous structures in vivo. The method integrates high-resolution SWI and anatomical knowledge derived from T1-weighted images. We investigate the ability of this technique to quantify vessels in the brain and apply it to an analysis of vessel density (VD) in the hippocampus in patients with neocortical epilepsy and MTLE.

Key Points

- Vessels were segmented in the hippocampus from high-resolution SWI images
- No significant difference in hippocampus symmetry was detected
- Significant changes in vessel symmetry in the hippocampus were detected in patients with mesial temporal lobe epilepsy

2 | MATERIALS AND METHODS

2.1 | Participants

Patients with epilepsy, between the ages of 18 and 78 years, were referred for 7-T imaging by their epileptologist (M.C.F. and L.V.M.). Inclusion criteria for this analysis required epilepsy patients to (1) have suspected seizure onset in the temporal lobe (MTLE), or other forms of focal epilepsy from the neocortex, as revealed by their clinical history, seizure semiology, and/or EEG data; (2) have standardized epilepsy protocol 1.5-T or 3-T MRI scans that were read as MRI-normal, that is, without epileptogenic lesions, by a neuroradiologist (B.N.D.); and (3) have no contraindications to 7-T MRI. Institutional review board approval for human research was obtained for this study, and written, fully informed consent was given by each participant prior to enrollment. A total of 17 MTLE patients (10 female; mean age = 37 ± 15 years), underwent scanning for the present study, as well as 17 neocortical patients (10 female, age = 37 ± 13 years), selected for similar age and gender, and 17 age- and gender-matched normal controls (10 female, mean age = 37 ± 13 years; Table 1). All MTLE patients recruited to participate in 7-T research on epilepsy patients with MRI-normal clinical scans were analyzed. Control volunteers were included if they had no contraindications to 7-T MRI and self-identified with no history of seizure or epilepsy. From neocortical patients, seizure onset was suspected to be focal (n = 10, including nine frontal and one parietal) or multifocal (n = 7).

TABLE 1 Participant demographics

	MTLE	Neocortical	Healthy controls
Number of subjects	17	17	17
Male	7	7	7
Female	10	10	10
Age, y ± SD	37 ± 15	37 ± 13	37 ± 13

Abbreviations: MTLE, mesial temporal lobe epilepsy; SD, standard deviation.

Additional clinical information is provided in supplementary Tables S1 and S2.

2.2 | Data acquisition

All imaging was performed on a 7-T whole-body scanner (Magnetom, Siemens Healthcare). A SC72CD gradient coil (max slew rate = 200 T/m/s, G_{max} = 70 mT/m) was used with a single channel transmit and a 32-channel receive head coil (Nova Medical). The patients were scanned using a 90-minute epilepsy MRI protocol, and qualitative analysis of the data has been reported.[34] For this analysis, we made use of the T1-weighted (MP2RAGE[35]) sequence (time of acquisition [TA] = 7:26, voxel size = 0.8 × 0.8 × 0.8 mm^3, field of view = 255 × 183 mm^2, repetition time [TR] = 6000 milliseconds, echo time [TE] = 5.1 milliseconds, inversion time [TI]1/TI2 = 1050/3000 milliseconds, flip angle [FA]1/FA2 = 5°/4°, matrix = 282 × 146, Bandwidth [BW] = 130 Hz/pixel, iPAT = 3) and the SWI sequence (TA = 7:30, voxel size = 0.2 × 0.2 × 1.5 mm^3, TR = 23 milliseconds, TE = 14 milliseconds, FA = 12°, matrix = 1024 × 832, BW = 150 Hz/pixel, image acceleration factor [iPAT] = 3).

2.3 | Vessel tracing

The protocol developed to automatically detect potential venous structures from the acquired data is illustrated in Figure 1. Uniform denoised (UNIDEN) images were produced from the MP2RAGE acquisitions (Figure 1A), and minimum intensity projection (mIP) images through five contiguous slices were produced from the magnitude of the SWI acquisition (Figure 1B). Masks were created using cortical, subcortical, and white matter volumetric segmentation of the brain in FreeSurfer v6.0 (http://surfer.nmr.mgh.harvard.edu, Massachusetts General Hospital). The UNIDEN image and associated mask were coregistered to the SWI image using SPM 12 software (www.fil.ion.ucl.ac.uk, Wellcome Center for Human Neuroimaging). The vessel tracing algorithm also utilized a volumetric segmentation of the hippocampus created in FreeSurfer (Figure 1D). The components of the segmentation comprising the

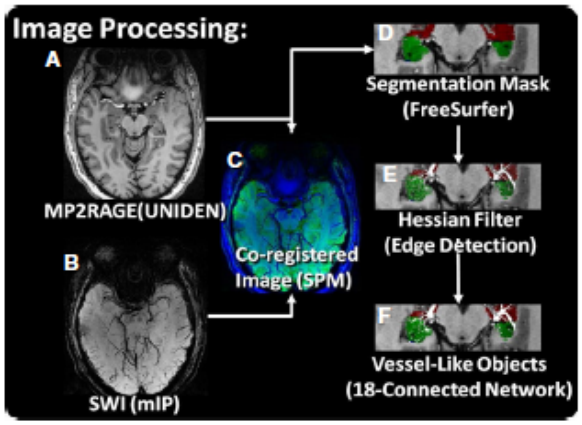

FIGURE 1 Image processing. A-C, The uniform denoised (UNIDEN) reconstruction of the MP2Rage image (A) and the susceptibility-weighted imaging (SWI) minimum intensity projection (mIP) image (B) were coregistered (C; MP2RAGE, green; SWI, blue). D, A segmentation of the hippocampus was used to mask the SWI with all components combined to make a right and left hippocampus mask. E, F, A Hessian edge detection filter was used to detect the ridges (E), which were linked on an 18-connected network (F). SPM, Statistical Parametric Mapping

hippocampus were combined to create a mask of the desired region of interest (ROI).

The mIP images were processed to detect potential venous structures based on the methods of Frangi and Steger[32,33] detection and segmentation implemented in MATLAB (MathWorks). Vessel enhancement was performed by finding the eigenvalues of the Hessian matrix and extracting the principle direction.[32] The results were masked using the combined hippocampal segmentation to include only the ROI (Figure 1E). The resulting three-dimensional datasets were linked along an 18-connected network through the nearest neighbors. Individual objects were characterized using the *bwlabel* function in MATLAB. Resultant networks excluded objects with a connected length of <4 voxels (Figure 1F). A consistent threshold was used for all analysis. The scripts used to produce this analysis are available upon reasonable request to the corresponding author.

2.4 | Verification

The vessel tracing protocol was validated against manually traced vessels across 13 noncontiguous axial mIP slices of a control SWI image representing the brain from the basal ganglia to the vertex. The manual tracings were performed with Osirix Image analysis software (Pixmeno). For comparison, the vessel tracing protocol was applied to the same slices, constrained by a mask containing a volumetric segmentation of white matter and gray matter. The manual and automatic vessel tracings were compared, and for the purposes of this analysis, the manual segmentations were

defined to be the gold standard manual positive results. The vessels detected on both the manual and automatic vessel tracing protocol were defined as true-positive (TP) results, and the venous structures detected on the manual segmentation but missed on the automatic tracing were defined as false-negative (FN) results. Finally, structures that were visible on the automatic tracing but absent from the manual tracing were defined as false-positive (FP) results based on the manual results (manual FPs [mFPs]) for the purpose of this calculation. True negatives (TNs), regions that were not marked in both the manual segmentation and the automated segmentation, constituted the majority of the image but were not segmented into objects or quantified.

Sensitivity of the automatic object segmentation was calculated using Equation 1:

$$\text{Sensitivity} = \frac{\text{TP}}{\text{TP} + \text{FN}} \tag{1}$$

Positive predictive value (PPV) was calculated using Equation 2:

$$\text{PPV} = \frac{\text{TP}}{\text{TP} + \text{FP}} \tag{2}$$

Sensitivity and PPV were calculated for each slice, and for the overall set of 13 slices based on the manual segmentation gold standard.

To evaluate the manual markings used as our standard, we randomly selected 20% of the mFPs identified through comparison of the manual and automatic tracings and evaluated the six slices surrounding the marking. The mFP was then classified as either an *accurate segmentation* (ie, an in-plane or through-plane visualization of a vessel that was missed by the manual segmentation and captured by the automatic segmentation) or a *false segmentation* (ie, noise or other image feature not identifiable as a vessel that was captured by the automatic segmentation).

Finally, TP voxels (TPv), TN voxels (TNv), FP voxels (FPv), and FN voxels (FNv) were identified using a voxelwise comparison of the manual and automatic segmentations. From these values, a voxelwise sensitivity, specificity, PPV, and the FP rate (FPR) were calculated.

2.5 | VD analysis of the hippocampus

HV for each subject was the total volume of the voxels contained within the volumetric segmentation of the T1-weighted images. This was calculated by determining the total number of voxels contained within each segmentation and multiplying by the acquired voxel volume. The same volumetric segmentations were used as the mask to demarcate the ROI for the automatic vessel tracing. The VD on both the left and right was estimated by calculating vessel volume (VV) as the total number of voxels traced in each ROI scaled by the voxel volume and dividing by HV (Equation 3).

$$\text{VD} = \frac{\text{VV}}{\text{HV}} \tag{3}$$

To explore left/right asymmetry, an asymmetry index (AI; Equation 4) and absolute asymmetry index (|AI|; Equation 5) were calculated for both HV (AI_v) and VD (AI_d). For the calculation of AI_v and AI_d, R represents HV or VD in the right ROI and L represents HV or VD in the left ROI.

$$\text{AI} = \frac{(R-L)}{\frac{1}{2}(R+L)} \tag{4}$$

$$|\text{AI}| = \frac{|(R-L)|}{\frac{1}{2}(R+L)} \tag{5}$$

To explore the correlation between HV and VD, HV and VD were calculated over the total hippocampus (left and right) for each subject and the Pearson product-moment correlation coefficient was calculated for each group (MTLE, neocortical, and control) and for the combined population of epilepsy patients (MTLE and neocortical).

2.6 | Statistical analysis

The HVs and VDs in the right and left hemispheres among MTLE, neocortical, and control groups were calculated. Patients and controls were compared using both $|AI_v|$ and $|AI_d|$, and between-group differences were calculated using a one-way analysis of variance (ANOVA) and Tukey post hoc test.

3 | RESULTS

3.1 | Tracing verification

The SWI mIP (Figure 2A,B) served as the substrate for both the manual tracing (Figure 2C,D) and the automated tracing (Figure 2E,F). The validation set contained a total of 1245 manually traced vessels used as the gold standard, and 1444 veins were identified by the automated method. A total of 1215 veins were concordant between the two methods. A total of 229 objects were labeled as veins by the automated method where none was indicated in the manual tracing (mFP). A total of 30 veins were only seen by manual tracing. The sensitivity of the automated tracing technique, calculated using Equation 1, is plotted in Figure 3A and ranged between 0.81 and 1.0, whereas the PPV of the method ranged between 0.63 and 1.00. Summary statistics give a sensitivity of 0.98 and a PPV of 0.84 (Figure 3B).

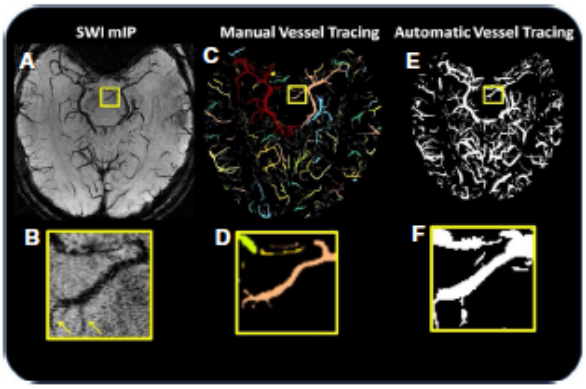

FIGURE 2 Comparison of manual and automated segmentation. A, Axial slice of the susceptibility-weighted imaging (SWI) minimum intensity projection (mIP). B, A magnification of the mIP vessels highlighted in the yellow box in A. C, Manually segmented vessels. D, A magnification of the manual segmentation highlighted in the yellow box in C. E, The result of automated vessel tracing. F, A magnification of the automatic segmentation highlighted in the yellow box in E. The arrows in B indicate that the automatic segmentation produced accurate segmentations of some manual false-positive vessels (ie, vessels that were identified in the automated segmentation but not in the manual segmentation)

3.2 | Analysis of FPs

Of the mFPs reexamined (approximately 20% of the 229 of the mFPs), three of 46 (6.5%) objects were classified as false segmentations, and the remaining 43 of 46 (93.5%) were classified as accurate segmentations (an example is given in Figure 2). Of the accurate segmentations, 27 of 43 (62.8%) were fully visible in the plane of the image, 13 of 43 (30.2%) were partially visible in the plane of the image but more fully visible in the slice immediately above or below the plane of the marked image, and three of 43 (7.0%) were vessels running essentially perpendicular to the plane of the image, identified as points of susceptibility that persist through five or more slices.

3.3 | Voxelwise validation

A voxelwise comparison between the manual and automatic tracings evaluated 6 202 326 voxels located within the brain mask over the 13 slices. The sensitivity of the automated technique compared to the manual segmentation was found to be 0.89 (TPv = 1 053 405, FNv = 131 345), and the specificity was found to be 0.96 (TNv = 4 805 978, FPv = 211 598). Thus, the PPV was 0.83, and the false discovery rate was 0.04.

3.4 | Comparison between MTLE, neocortical, and control groups

The total HVs in the MTLE (mean = 2.1 ± 0.5 cm^3), neocortical (mean = 2.4 ± 0.2 cm^3), and control groups (mean = 2.7 ± 0.3 cm^3) ranged between 1.8 and 3.5 cm^3, with the lowest HV found in a patient with left temporal epilepsy, and the largest in a control.

Individually calculated AI_v and AI_d are reported in the supplementary information (Tables S1 and S2). In aggregate, there was little asymmetry in the control population in total HV (mean $|AI_v|$ = 0.065 ± 0.04, median = 0.06). Although the mean volume asymmetry was slightly higher than controls in both neocortical (mean $|AI_v|$ = 0.066 ± 0.06, median = 0.05) and MTLE ($|AI_v|$ = 0.135 ± 0.15, median = 0.05) groups, the medians were slightly lower, as shown in Figure 4. A one-way ANOVA resulted in no significant differences between the group means.

A

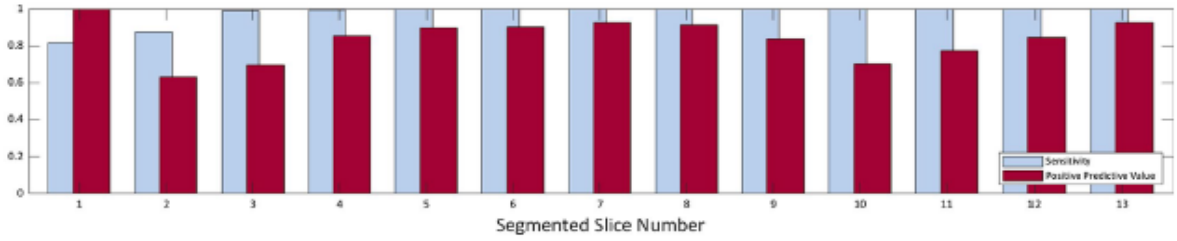

B

	# True Positive	# False Positive	# False Negative	Sensitivity	Positive Predictive Value
Overall	1215	229	30	0.98	0.84

FIGURE 3 A, Slice-by-slice sensitivity and positive predictive value (PPV) calculation of the automated method against the manual gold standard. B, Overall sensitivity and PPV of automatic vessel tracing

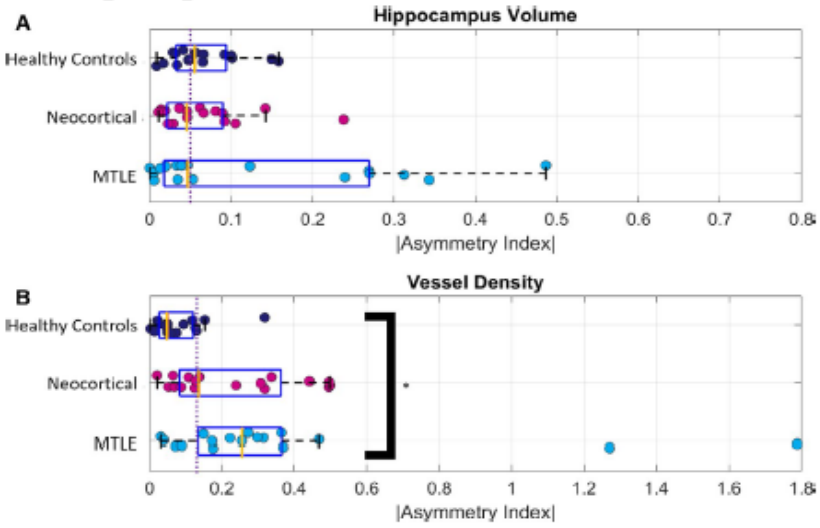

FIGURE 4 Asymmetry of hippocampal volume and vessel density. The purple line in each part represents the median value for all groups. A, The mean asymmetry of hippocampus volume is not significantly different between mesial temporal lobe epilepsy (MTLE) and neocortical patients and controls, although there is more variability in the epilepsy patients. B, The asymmetry in vessel density is significantly higher and MTLE than in controls $*P < .04$. Median for each group is indicated with an orange bar

VD was also highly symmetric in controls (mean $|AI_d| = 0.080 \pm 0.076$, median = 0.050), whereas average VD asymmetry was greater in neocortical (mean $|AI_d| = 0.23 \pm 0.17$, median = 0.14) and MTLE (mean $|AI_d| = 0.37 \pm 0.46$, median = 0.26) patients. A one-way ANOVA indicated significant differences in the group means ($P < .02$), and Tukey post hoc test indicated that this result was driven by a significant difference between MTLE and controls groups ($P < .05$) in VD asymmetry. No other significant differences were indicated.

In all cases, the asymmetry reflected a lower VD in the hippocampus ipsilateral to the suspected seizure onset zone when compared to the contralateral hippocampus (Tables S1 and S2). This result is shown for a control and an epilepsy patient over several slices of the hippocampus in Figure 5.

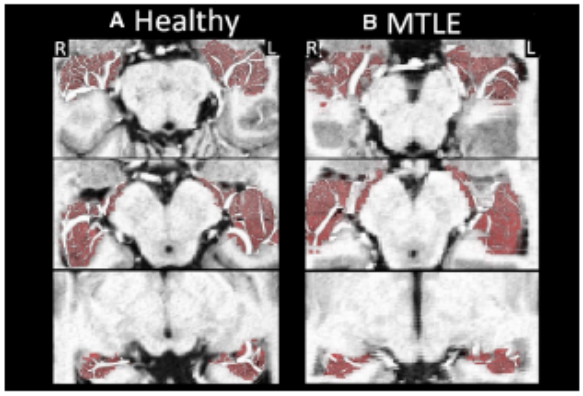

FIGURE 5 Vessels in the hippocampus over three axial slices for (A) a control and (B) a patient with mesial temporal lobe epilepsy (MTLE) of suspected left (L) onset. The radiological right hippocampus (R) is located on the left side of the image

3.5 | Correlation between VD and HV

Weak, insignificant positive correlation between VD and HV was found in all groups. The correlation in the control group was $r_{15} = 0.02$, $P = .93$; the correlation in the neocortical group was $r_{15} = 0.20$, $P = .43$; the correlation in the MTLE group was $r_{15} = 0.31$, $P = .21$. Over the combined group of epilepsy patients (neocortical and MTLE), there was a weak but significant correlation between VD and HV ($r_{32} = 0.33$, $P = .04$).

4 | DISCUSSION

The present study utilized SWI to assess changes in hippocampal venous vasculature in vivo, and results show a decrease in VD in the hippocampus in patients with MTLE who have nonlesional clinical MRI.

4.1 | Comparison between manual and automatic vessel tracings

Our analysis demonstrates a high level of agreement between the manual and automatic tracings. The method was less sensitive in slices in the more inferior brain, closer to the paranasal sinuses and basal ganglia. The PPV of the automatic object segmentation against the manual tracing was increasingly accurate from the basal ganglia to the vertex. The net PPV was calculated to be 0.84, meaning that approximately one of six objects traced automatically was not identified as a vessel during the manual marking (mFP). An examination of 46 (20%) of the mFPs revealed that three (7%) of the vessels were falsely segmented by the algorithm. By applying the same accurate segmentation and false segmentation rates to the rest of the sample, the

number of FPs (false segmentations) could be corrected to 15, whereas the number of TPs (accurate segmentations) could be corrected to 1429. Finally, the number of FNs would remain unaffected (30 total).

The voxelwise analysis produced values for sensitivity and PPV that were lower than the object-based validation. In addition to the voxels contained in the 229 mFP objects identified by the algorithm (Figure 2D,F), the boundaries identified on the manual and automatic vessel segmentations are not identical; thus, objects identified as mTPs on the automatic segmentation contain voxels that are TPv, FPv, and FNv, reducing the overall specificity and PPV.

Although the majority of structures (and voxels) were common to both the automatic and manual vessel segmentation techniques, each protocol also uniquely identified a set of vessel structures. The object-based segmentation revealed that manual segmentation was more accurate in regions near the sinuses or where low overall signal rendered SWI less reliable but where it was possible to manually interpret the image through noise. However, the automatic segmentation technique did not suffer from inconsistencies due to manual rater fatigue and was likely better able to combine information across multiple imaging planes to identify vessels across slices, particularly closer to the vertex.

4.2 | Volume asymmetry

Hippocampal asymmetry, rather than overall hippocampus volume, is a more common qualitative metric used in conjunction with hyperintensity on fluid-attenuated inversion recovery images to radiologically identify hippocampal sclerosis.[36] An analysis of the quantitative volumetric AI_v in neocortical, MTLE, and control groups reveals only minor, nonsignificant changes to mean asymmetry in both groups of epilepsy patients when compared to controls (Figure 4A). This analysis was performed on data acquired from patients whose prior clinical scans were interpreted as nonlesional, in whom no significant qualitative hippocampal asymmetry had been described. Thus, this result of minimal quantitative volumetric hippocampal asymmetry in patients with neocortical epilepsy and MTLE is consistent with the initial referral criteria.

4.3 | VD asymmetry

Quantitative vessel analysis using SWI mIPs in MTLE and neocortical epilepsy did reveal structural indicators of the presence of disease even in the absence of a qualitative identification of volumetric hippocampal sclerosis. A qualitative examination of the 7-T structural images for the two MTLE patients with high AI (Figure 4, |AI| = 1.27 and 1.79, Table 1), revealed suggestions of hippocampal asymmetry and bilateral hippocampal sclerosis not visible in their clinical scans. This appears consistent with previous work investigating the hippocampus, and in particular the CA1 subfield and the cornu ammonis as a whole, which indicates that in epilepsy these regions are particularly susceptible to deterioration.[6–9] In temporal lobe epilepsy, changes in permeability of the blood-brain barrier in the hippocampus have been reported, likely associated with the development of the inflammatory processes that induce glial hypertrophy, proliferation, and neuronal death.[12–14] It therefore follows that changes to vascular structures may play a significant role in, or may result from, epileptic pathology.

The abnormal vasodynamics coupled with a reduction in functional vessels might further contribute to microscopic hypoxia and ictal neurodegeneration.[37,38] Thus, ongoing seizures may eventually involve structures and vasculature in the hippocampus even when the region is not implicated as a primary epileptogenic zone. Patients without suspected seizure onset zones in the mesial temporal lobes (neocortical) showed a mean asymmetry (mean $|AI_d| = 0.23 \pm 0.17$) greater than controls (mean $|AI_d| = 0.08 \pm 0.76$), but the post hoc test did not indicate significance. Approximately half (9/17) of the neocortical patients had $|AI_d| > 0.13$, which more closely resembled MTLE patients ($|AI_d| > 0.13$ in 13/17 patients) than controls ($|AI_d| > 0.13$ in 2/17 patients). This suggests that in approximately half of the epilepsy patients without EEG or clinical symptoms indicating a mesial temporal seizure onset zone (neocortical), there may be some degree of hippocampal involvement.

4.4 | Correlation between HV and VD

For all subjects, the voxelwise vessel segmentation was normalized by the HV to produce VD to minimize the correlation between the metrics. In controls, the correlation between HV and VD was very weak and nonsignificant. However, for epilepsy patients, a weak positive correlation was detected between HV and VD in both groups. This correlation did not achieve significance for the sample size. However, when the correlation between HV and VD was analyzed for all epilepsy patients (MTLE and neocortical), a weak but significant correlation was identified. This suggests that, in the presence of pathology, both hippocampus volume and VD are decreased, and that sclerotic tissue is drained by disproportionately fewer intact vessels.

Although differences in the symmetry of hippocampus volumes were not identified, the analysis may have been limited by the segmentation tool used. FreeSurfer may not be capable of providing segmentations with sufficient accuracy and precision to detect real, but small, alterations in hippocampus volumes in the 7-T datasets evaluated here.

Future work evaluating a larger sample size with more precise segmentation tools could explore the correlation between VD and HV and indicate where a decrease in VD may identify hippocampal pathology before changes in HV are detected.

4.5 | Hippocampal vasculature in previous ex vivo work

Although histochemical markers of increased vessel formation would seem to be in conflict with our finding of reduced VD ipsilateral to the suspected epileptogenic zone,[15] other ex vivo experiments have shown diminished histochemical labeling of alkaline phosphatase (AP) in CA1 subfields that exhibit sclerosis.[23] AP is a marker of endothelial cells in the blood-brain barrier, so gross reduction is a marker of lower concentrations of AP-positive vessels. Additionally, because AP activity appears to be altered during induced seizure activity in rats, abnormalities in the AP genetic structure may prompt epileptic activity through perturbation of the role of AP in regulating γ-aminobutyric acid (GABA) synthesis, leading to alterations in GABAergic regulation.[23,24] High-magnification light and electron microscopy of resected specimens also suggests that blood vessels are diminished within epileptogenic zones within human hippocampi. Collectively, these findings appear to suggest that prior ex vivo results showing increased vascular markers have identified not only functional vessels providing drainage but also collapsed and atrophic vessel fragments in the labeling. When such vessel damage was taken into account, active vasculature was actually significantly reduced in sclerotic hippocampi.[25,26]

The presence of atrophic blood vessels in sclerotic hippocampi suggests that a reduction of "normal" vasculature in this region is a characteristic of MTLE. This local reduction in functional veins may be representative of aberrant vasogenesis and is consistent with our imaging results identifying a decrease in structures carrying deoxygenated blood in the hippocampus. However, more imaging studies with larger sample sizes and validation with resected tissue will be necessary to truly ascertain the pathophysiological processes underlying these vascular differences.

4.6 | Additional limitations and future directions

Susceptibility-weighted imaging emphasizes the incoherent signals in each voxel and the phase accumulation due to local sources of magnetic susceptibility, leading to a magnification of the effect of small veins in the image.[28] Thus, we would expect an overemphasis on small vessels as detected by both the manual and automatic tracing methods.

Another limitation of the technique is the potential conflation of veins with other sources of T2*-shortening. In the validation set, approximately three of the 46 "FPs" identified through comparison between the manual tracing and the automatic segmentation we considered to be false segmentations, that is, segmentations that, upon visual inspections of the image, were considered to unlikely to be vessels. Other image features, such as calcifications, and hemosiderin appear dark on SWI. The filters designed by Frangi and Steger were constructed to detect long edges, such as roads and vessels. Thus, when applied to calcification or hemosiderin, punctate sources of susceptibility will not be segmented. However, when the impact of these features on the image becomes long, thin, and more vessellike, the segmentation tool will detect them.

The proximity of veins to other susceptible structures, such as air and bone, including near the skull base, may challenge the detection of small structures using this technique. This may be problematic when analyzing veins near low signal structures, leading to impaired detection accuracy in regions affected by both radiofrequency and main field inhomogeneity.

Previous work has shown that volume loss in selective hippocampal subfields is correlated to epilepsy.[39–41] It has been shown that different parts of the hippocampus show different levels of resistance to disruption in perfusion, with the CA1 region known to be particularly sensitive, whereas CA2 and CA3 are thought to be particularly resistant.[42] Thus, it may be possible that this change in VD is also associated with particular hippocampal subfields. By acquiring high-resolution SWI of sufficient quality to permit subfield segmentation in addition to the vessel segmentation, it may be possible to further localize and characterize this change in subfield vasculature as it relates to MTLE.

Finally, only group differences in asymmetry were evaluated, due to the limited sample size. Future work, on a larger sample size, would power a direct comparison of HV and VD that could highlight bilateral pathology in both MTLE and neocortical epilepsy patients, which is lost in the self-normalization intrinsic to the AI calculation. The analysis of VD symmetry in patients with neocortical epilepsy did not yield results significantly different from those of controls. There was a wider distribution of asymmetry in neocortical patients when compared to controls. High VD asymmetry among neocortical patients may implicate a wider seizure network. Future work could include a larger patient population, seizure duration, seizure severity, and an analysis of refractoriness alongside VD asymmetry in the hippocampus and possibly throughout the brain. Further validation of VD asymmetry as a biomarker through imaging and histology may help to provide a means of identifying patients who are more likely to be refractory to medications, to target electrode placement surgically during intracranial monitoring to evaluate more

elaborate seizure networks, and to guide interventions such as responsive neurostimulator placement.

This experiment aggregates VD over the entire hippocampus. Measurement of this metric as part of a comprehensive epilepsy imaging protocol may permit us to follow and assess structural changes associated with MTLE and eventually prevent or ameliorate the progression of neuronal damage in patients via the administration of targeted pharmacotherapy.[38]

5 | CONCLUSIONS

We introduce and validate a novel method of venous structure detection and report in vivo evidence of reduced functional vasculature in the hippocampus associated with MTLE. This feature is visible in patients with MTLE, even when qualitative and quantitative measures of hippocampal asymmetry show little volumetric difference between epilepsy patients and controls.

ACKNOWLEDGMENTS

The research reported in this article was supported by National Institutes of Health (NIH) National Institute of Neurological Disorders and Stroke R00 NS070821, NIH R01 MH109544, and US Department of Defense (DOD) W81XWH-18-ERP-IDA.

CONFLICT OF INTEREST

P.B. is a named inventor on patents relating to MRI and radiofrequency (RF) pulse design. The patents have been licensed to GE Healthcare, Siemens, and Philips International. P.B. receives royalty payments relating to these patents. P.B. is a named inventor on the patents "Slice-Selective Adiabatic Magnetization T2-Preparation (SAMPA) for Efficient T2-Weighted Imaging at Ultrahigh Field Strengths," "Methods for Producing a Semi-Adiabatic Spectral-Spatial Spectroscopic Imaging Sequence and Devices Thereof," and "Semi-Adiabatic Spectral-Spatial Spectroscopic Imaging." These patents have been filed through Mount Sinai Innovation Partners; they remain unlicensed, there is no discussion to license them in the near future, and there are consequently no royalties resulting from them. R.E.F. is a named inventor on patents relating to MRI and RF pulse design, "Semi-Adiabatic Spectral-Spatial Spectrospatial Imaging (SASSI)" and "Semi-Adiabatic Matched Phase Spin Echo Power Independent of the Number of Pulses (SEAMS PINS)." She does not receive financial compensation related to these patents. The remaining authors report no conflict of interest concerning the materials or methods used in this study or the findings specified in this paper. We confirm that we have read the Journal's position on issues involved in ethical publication and affirm that this report is consistent with those guidelines.

ORCID

Rebecca Emily Feldman https://orcid.org/0000-0001-8403-9807
Gaurav Verma https://orcid.org/0000-0002-7157-439X
Madeline Cara Fields https://orcid.org/0000-0003-0661-4153

REFERENCES

1. Ngugi AK, Bottomley C, Kleinschmidt I, et al. Prevalence of active convulsive epilepsy in sub-Saharan Africa and associated risk factors: cross-sectional and case-control studies. Lancet Neurol. 2013;12:253–63.
2. Bell GS, Sander JW. The epidemiology of epilepsy: the size of the problem. Seizure. 2001;10:306–14.
3. Murray CJ, Vos T, Lozano R, et al. Disability-adjusted life years (DALYs) for 291 diseases and injuries in 21 regions, 1990–2010: a systematic analysis for the Global Burden of Disease Study 2010. Lancet. 2012;380:2197–223.
4. WHO. Epilepsy: Epidemiology, Aetiology and Prognosis. Geneva, Switzerland: World Health Organization; 2001.
5. Belhocine M, deBoer H, Mandlhate C. Epilepsy in the WHO African Region: Bridging the Gap. Geneva, Switzerland: World Health Organization; 2004.
6. Crespel A, Coubes P, Rousset MC, et al. Immature-like astrocytes are associated with dentate granule cell migration in human temporal lobe epilepsy. Neurosci Lett. 2002;330:114–8.
7. Crespel A, Rigau V, Coubes P, et al. Increased number of neural progenitors in human temporal lobe epilepsy. Neurobiol Dis. 2005;19:436–50.
8. Rigau V, Morin M, Rousset MC, et al. Angiogenesis is associated with blood-brain barrier permeability in temporal lobe epilepsy. Brain. 2007;130:1942–56.
9. Meldrum B, Bruton C. Epilepsy. In: Adams J, Duchen L eds. Greenfield's Neuropathology. 5th ed. London, UK: Oxford University Press; 1992:1246–83.
10. Duncan JS, Sander JW, Sisodiya SM, Walker MC. Adult epilepsy. Lancet. 2006;367:1087–100.
11. So EL. Role of neuroimaging in the management of seizure disorders. Mayo Clin Proc. 2002;77:1251–64.
12. Ravizza T, Gagliardi B, Noe F, Boer K, Aronica E, Vezzani A. Innate and adaptive immunity during epileptogenesis and spontaneous seizures: evidence from experimental models and human temporal lobe epilepsy. Neurobiol Dis. 2008;29:142–60.
13. Ravizza T, Noe F, Zardoni D, Vaghi V, Sifringer M, Vezzani A. Interleukin converting enzyme inhibition impairs kindling epileptogenesis in rats by blocking astrocytic IL-1beta production. Neurobiol Dis. 2008;31:327–33.
14. Oby E, Caccia S, Vezzani A, et al. In vitro responsiveness of human-drug-resistant tissue to antiepileptic drugs: insights into the mechanisms of pharmacoresistance. Brain Res. 2006;1086:201–13.
15. Vigneau-Roy N, Bernier M, Descoteaux M, Whittingstall K. Regional variations in vascular density correlate with resting-state and task-evoked blood oxygen level-dependent signal amplitude. Hum Brain Mapp. 2014;35:1906–20.
16. Leal-Campanario R, Alarcon-Martinez L, Rieiro H, et al. Abnormal capillary vasodynamics contribute to ictal neurodegeneration in epilepsy. Sci Rep. 2017;7:43276.
17. Pitkanen A, Lukasiuk K. Molecular and cellular basis of epileptogenesis in symptomatic epilepsy. Epilepsy Behav. 2009;14(Suppl 1):16–25.

18. Morin-Brureau M, Lebrun A, Rousset MC, et al. Epileptiform activity induces vascular remodeling and zonula occludens 1 down-regulation in organotypic hippocampal cultures: role of VEGF signaling pathways. J Neurosci. 2011;31:10677–88.
19. Morin-Brureau M, Rigau V, Lerner-Natoli M. Why and how to target angiogenesis in focal epilepsies. Epilepsia. 2012;53(Suppl 6):64–8.
20. Penfield W, Jasper H. Epilepsy and the Functional Anatomy of the Human Brain. London, UK: Churchill; 1954.
21. Haglund MM, Ojemann GA, Hochman DW. Optical imaging of epileptiform and functional activity in human cerebral cortex. Nature. 1992;358:668–71.
22. Tae WS, Joo EY, Kim JH, et al. Cerebral perfusion changes in mesial temporal lobe epilepsy: SPM analysis of ictal and interictal SPECT. Neuroimage. 2005;24:101–10.
23. Erakovic V, Zupan G, Varljen J, Laginja J, Simonic A. Altered activities of rat brain metabolic enzymes in electroconvulsive shock-induced seizures. Epilepsia. 2001;42:181–9.
24. Fonta C, Negyessy L, Renaud L, Barone P. Areal and subcellular localization of the ubiquitous alkaline phosphatase in the primate cerebral cortex: evidence for a role in neurotransmission. Cereb Cortex. 2004;14:595–609.
25. Alonso-Nanclares L, DeFelipe J. Alterations of the microvascular network in the sclerotic hippocampus of patients with temporal lobe epilepsy. Epilepsy Behav. 2014;38:48–52.
26. Kastanauskaite A, Alonso-Nanclares L, Blazquez-Llorca L, Pastor J, Sola RG, DeFelipe J. Alterations of the microvascular network in sclerotic hippocampi from patients with epilepsy. J Neuropathol Exp Neurol. 2009;68:939–50.
27. Haacke E, Xu Y, Cheng Y, Reichenbach J. Susceptibility weighted imaging (SWI). Magn Reson Med. 2004;52:612–8.
28. Liu S, Buch S, Chen Y, et al. Susceptibility-weighted imaging: current status and future directions. NMR Biomed. 2017;30:e3552.
29. Reichenbach JR, Barth M, Haacke EM, Klarhofer M, Kaiser WA, Moser E. High-resolution MR venography at 3.0 tesla. J Comput Assist Tomogr. 2000;24:949–57.
30. Ward PGD, Ferris NJ, Raniga P, et al. Combining images and anatomical knowledge to improve automated vein segmentation in MRI. Neuroimage. 2017;165:294–305.
31. Lesage D, Angelini ED, Bloch I, Funka-Lea G. A review of 3D vessel lumen segmentation techniques: models, features and extraction schemes. Med Image Anal. 2009;13:819–45.
32. Frangi AF, Niessen WJ, Vincken KL, Viergever MA, eds. Multiscale Vessel Enhancement Filtering. Berlin, Heidelberg, Germany: Springer; 1998.
33. Steger C. An unbiased detector of curvilinear structures. IEEE Trans Pattern Anal Mach Intell. 1998;20:113–25.
34. Re F, Delman B, Pawha P, et al. 7T MRI in epilepsy patients with previously normal clinical MRI exams compared against healthy controls. PLoS One. 2019;14:e0213642.
35. Marques JP, Kober T, Krueger G, van der Zwaag W, Van de Moortele PF, Gruetter R. MP2RAGE, a self bias-field corrected sequence for improved segmentation and T1-mapping at high field. Neuroimage. 2010;49:1271–81.
36. Ruber T, David B, Elger CE. MRI in epilepsy: clinical standard and evolution. Curr Opin Neurol. 2018;31:223–31.
37. Marinkovic S, Milisavljevic M, Puskas L. Microvascular anatomy of the hippocampal formation. Surg Neurol. 1992;37:339–49.
38. Farrell JS, Gaxiola-Valdez I, Wolff MD, et al. Postictal behavioural impairments are due to a severe prolonged hypoperfusion/hypoxia event that is COX-2 dependent. Elife. 2016;5:e193552.
39. Santyr BG, Goubran M, Lau JC, et al. Investigation of hippocampal substructures in focal temporal lobe epilepsy with and without hippocampal sclerosis at 7T. J Magn Reson Imaging. 2017;45:1359–70.
40. Peslova E, Marecek R, Shaw DJ, Kasparek T, Pail M, Brazdil M. Hippocampal involvement in nonpathological deja vu: subfield vulnerability rather than temporal lobe epilepsy equivalent. Brain Behav. 2019;8:e00996.
41. Kreilkamp BAK, Weber B, Elkommos SB, Richardson MP, Keller SS. Hippocampal subfield segmentation in temporal lobe epilepsy: relation to outcomes. Acta Neurol Scand. 2018;137:598–608.
42. Duvernoy H. The Human Hippocampus: An Atlas of Applied Anatomy. Munich, Germany: JF Bergmann Verlag; 1988.

SUPPORTING INFORMATION

Additional supporting information may be found online in the Supporting Information section.

How to cite this article: Feldman RE, Marcuse LV, Verma G, et al. Seven-tesla susceptibility-weighted analysis of hippocampal venous structures: Application to magnetic-resonance–normal focal epilepsy. *Epilepsia*. 2020;61:287–296. https://doi.org/10.1111/epi.16433

Appendix 3: ISMRM Abstract and Poster

2011

An MRI traumatic brain injury case study at 7 Tesla: pre- and post-injury structural network and volumetric reorganization and recovery

Stephanie S. G. Brown[1,2], Kristen Dams-O'Connor[3], Priti Balchandani[4], and Rebecca E. Feldman[5]
[1]Department of Psychiatry, University of Cambridge, Cambridge, United Kingdom, [2]Biomedical Engineering and Imaging Institute, Icahn School of Medicine at Mount Sinai / University of Cambridge, New York, NY, United States, [3]Brain Injury Research Centre, Icahn School of Medicine at Mount Sinai, New York, NY, United States, [4]Biomedical Engineering and Imaging Institute, Icahn School of Medicine at Mount Sinai, New York, NY, United States, [5]Department of Computer Science, Mathematics, Physics, and Statistics, University of British Columbia, Kelowna, BC, Canada

Synopsis

This case study investigates the structural effects of traumatic brain injury for the first time using pre-injury and post-injury 7 Tesla MRI longitudinal data. We report findings of initial volumetric changes, decreased structural connectivity and reduced microstructural order that appear to return to baseline 8 months post-injury, suggestive of long-term plasticity and recovery.

Introduction: A significant limitation of many studies examining traumatic brain injury (TBI) is the scarcity of pre-injury data. In present case study, we aimed to leverage ultra-high field MRI over multiple acquisition timepoints to examine how a right parietal bone impact affected gross brain structure, subcortical volumetrics, microstructural order and connectivity longitudinally.
Methods: An adult female patient was knocked over by a car, causing a loss of consciousness for several seconds. The post-injury CT scan showed subcutaneous soft tissue swelling over the right parietal bone. The patient had undergone two scanning sessions at 7 Tesla prior to the head injury as a healthy control research participant. Two more scans were acquired post-injury. The scan dates were as follows: February 2016, January 2017, January 2018 and August 2018. Included in each protocol was a T1-weighted Magnetization Prepared 2 Rapid Acquisition Gradient Echo Echo (MP2RAGE) (1), a T2-weighted Turbo Spin Echo (TSE), and a diffusion MRI (dMRI). The MP2RAGE high spatial resolution (1) voxel size was 0.8 mm isotropic, TR/TE = 6000/3.2 ms and TI1(81)/TI2(82) = 1050(5^s)/3000(4^s) ms. Two TSE structural images were obtained at high in-plane resolution (0.4 x 0.4 mm2) and a slice thickness of 2 mm. TR/TE = 6900/69 ms, and θ = 150°. The first T2-TSE was obtained in a coronal-oblique orientation where the imaging plane was aligned perpendicular to the long axis of the hippocampus. The second T2-TSE was obtained in an axial orientation, the imaging plane aligned along the axis connecting the anterior commissure and the posterior commissure (AC-PC). Diffusion MRI were also acquired at each scan timepoint, using a single-shot spin-EPI sequence aligned axially with an isotropic resolution of 1.05 mm and TR/TE = 6900/87 ms. The diffusion sequence was a paired acquisition with reversed phase encoding in the AP/PA direction. Each pair had 64 diffusion encoding directions (b=1200 s/mm2) and 4 unweighted scans (b=0 s/mm2). The FreeSurfer 'recon-all' pipeline (version 6.0) (2) was used to process the T1-weighted structural data at submillimetre resolution (3). Hippocampal subfield (4) and amygdala subnuclei segmentation (5) were also carried out using FreeSurfer. A multispectral segmentation approach was used, utilizing both the T1-weighted and T2-weighted images, leveraging the enhanced resolution of the T2-weighted image to provide additional anatomical information. Structural connectomes at different timepoints were compared by custom functions that performed elementwise subtraction of the matrices in MATLAB. To determine a streamline threshold of the connectome with an acceptable level of variability, mean matrix co-efficients of variation were calculated for the following streamline thresholds: 25, 50, 100, 200, 400, 800, 1600, 3200, 6400, 12800 and 25600 (Fig. 1). Actual streamline thresholding was set at 15000, discarding edges consisting of streamline bundles with less density than the threshold. Volumetrics, fractional anisotropy (FA) and connectivity were analyzed at each of the 4 time points and compared.
Results: The subcortical segmentation of the amygdala nuclei and hippocampal subfields did not reveal any clear changes between the scanning timepoints (Fig. 2). At post-injury timepoint 1, the right and left hemispheric brain segmentation revealed lower cortical grey matter and cerebral white matter volume compared to other scanning timepoints. No change was apparent in ventricle volume (Fig. 3). Mean post-injury structural connectivity displayed widespread reduction in the network connection density compared to mean pre-injury data. A comparison between the mean pre-injury connectome and the two post-injury matrices was then carried out, to investigate if changes to the patient's structural connectivity post-TBI was consistent over time. The results showed that at post-injury timepoint 1, connection density was extensively reduced, but this decrease in connectivity was much diminished by post-injury timepoint 2 (Fig. 4). Concurrent with the changes in the structural connectome and volumetrics, fractional anisotropy (FA) of the cerebral white matter was markedly reduced in both hemispheres in the first scan following the head trauma. In both the left and right hemispheres, the final timepoint scan revealed a subsequent increase of FA to levels similar to those pre-injury (Fig. 5).
Discussion: Here, our case data show that the post-traumatic injury brain exhibits widespread alterations to the cortical grey matter and cerebral white matter volume. Additionally, white matter connectivity displays generalized decreased connection strength across the network, both in terms of connection density and microstructural order of the tissue. Interestingly, structural changes attributed to head trauma are no longer evident by the final scanning timepoint, suggestive of long-term plasticity and recovery.
Conclusion: This case study investigates the structural effects of traumatic brain injury for the first time using pre-injury and post-injury 7 Tesla MRI longitudinal data. We report findings of initial volumetric changes, decreased structural connectivity and reduced microstructural order that appear to return to baseline 8 months post-injury.

Acknowledgements

No acknowledgement found.

References

1. Marques JP, Gruetter R. New developments and applications of the MP2RAGE sequence--focusing the contrast and high spatial resolution R1 mapping. PLoS One 2013;8(7):e69294. doi: 10.1371/journal.pone.0069294 2. Fischl B, Salat DH, Busa E, Albert M, Dieterich M, Haselgrove C, van der Kouwe A, Killiany R, Kennedy D, Klaveness S, Montillo A, Makris N, Rosen B, Dale AM. Whole brain segmentation: automated labeling of neuroanatomical structures in the human brain. Neuron 2002;33(3):341-355. 3. Zaretskaya N, Fischl B, Reuter M, Renvall V, Polimeni JR. Advantages of cortical surface reconstruction using submillimeter 7 T MEMPRAGE. Neuroimage 2018;165:11-26. doi: 10.1016/j.neuroimage.2017.09.060 4. Iglesias JE, Augustinack, J.C., Nguyen, K., Player, C.M., Player, A., Wright, M., Roy, N., Frosch, M.P., Mc Kee, A.C., Wald, L.L., Fischl, B., and Van Leemput, K. A computational atlas of the hippocampal formation using ex vivo, ultra-high resolution MRI: Application to adaptive segmentation of in vivo MRI. Neuroimage 2015;115(117-137). 5. Saygin ZM, Kliemann D, Iglesias JE, van der Kouwe AJW, Boyd E, Reuter M, Stevens A, Van Leemput K, McKee A, Frosch MP, Fischl B, Augustinack JC, Alzheimer's Disease Neuroimaging I. High-resolution magnetic resonance imaging reveals nuclei of the human amygdala: manual segmentation to automatic atlas. Neuroimage 2017;155:370-382. doi: 10.1016/j.neuroimage.2017.04.046

Figures

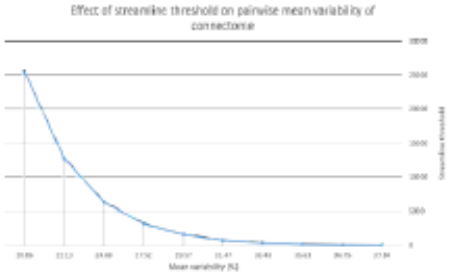

Fig. 1. Streamline threshold effect on variability of the connectome: averaged element-wise change of connectivity matrix between pre-injury timepoint 1 and pre-injury timepoint 2.

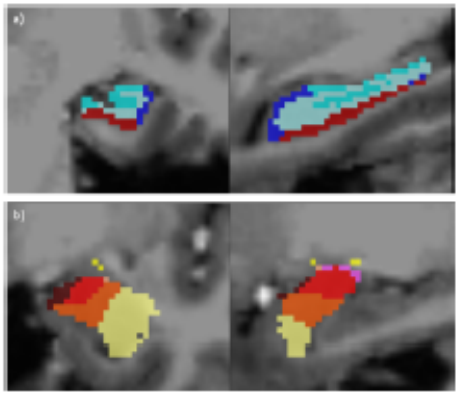

Fig. 2. a) Hippocampal subfield segmentation as performed by FreeSurfer, into dentate gyrus, subicular complex, CA1 and CA3/4 and b) amygdala subnuclei segmentation as performed by FreeSurfer into the basal, lateral, accessory basal, central, cortical and medial nuclei.

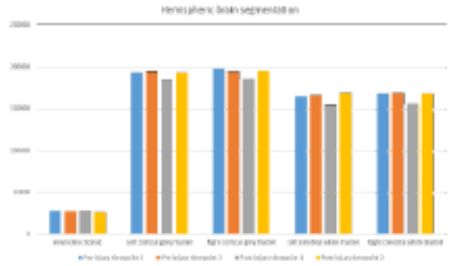

Fig. 3. Ventricle volume and hemispheric volumes of the cortical grey matter and cerebral white matter at each scanning timepoint.

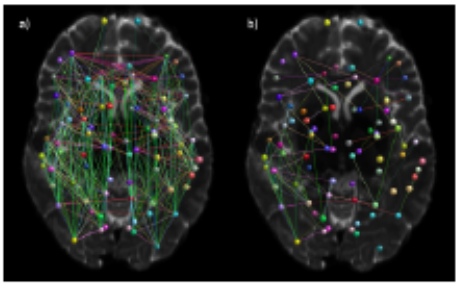

Fig. 4. a) Decrease in structural network connectivity at post-injury scanning timepoint 1 compared to mean pre-injury scans and b) decreased structural network connectivity at post-injury scanning timepoint 2 compared to mean pre-injury connectivity.

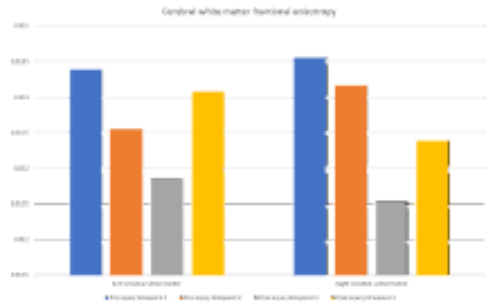

Fig. 5. Fractional anisotropy of hemispheric cerebral white matter at each scanning timepoint.

An MRI traumatic brain injury longitudinal case study at 7 Tesla: pre- and post-injury structural network and volumetric reorganization and recovery

Stephanie S. G. Brown*[1], Kristen Dams-O'Connor[2,3], Eric Watson[2], Priti Balchandani[4], Rebecca E. Feldman[5]

*e-mail: sb2403@medschl.cam.ac.uk

[1]Cambridge Intellectual & Developmental Disabilities Research Group, Department of Psychiatry, University of Cambridge, Cambridge, United Kingdom
[2]Department of Rehabilitation and Human Performance, Brain Injury Research Center, Icahn School of Medicine at Mount Sinai, New York, NY, United States
[3]Department of Neurology, Icahn School of Medicine at Mount Sinai, New York, NY, United States
[4]Translational and Molecular Imaging Institute, Icahn School of Medicine at Mount Sinai, New York, NY, United States
[5]Department of Computer Science, Mathematics, Physics, and Statistics University of British Columbia, Kelowna, BC, Canada

Introduction

Traumatic brain injury (TBI) is a leading cause of disability worldwide, particularly in young and military populations, with well-documented links to psychiatric and neurodegenerative pathology. A significant limitation of studies examining mild traumatic brain injury (mTBI) is the unavailability of pre-injury data. In the present case study, we leveraged multi-modal 7 Tesla MRI data acquired at two timepoints prior to mTBI, and two timepoints post-injury, to examine how a parietal impact affects gross brain structure, subcortical volumetrics, microstructural order and connectivity.

Results and Discussion

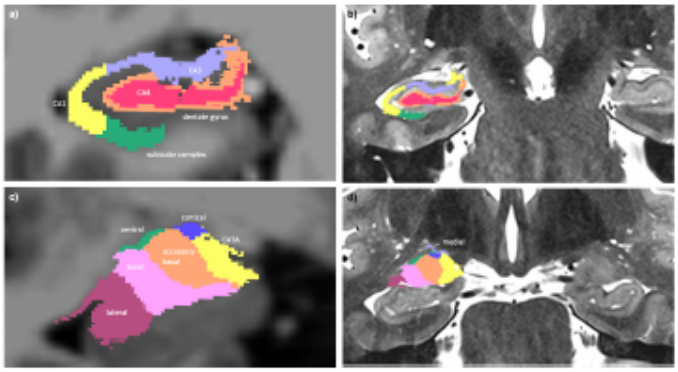

Figure 1. a) Multi-spectral hippocampal subfield segmentation (CA1, CA3, CA4, dentate gyrus and subicular complex) with underlay of axial T1-weighted data b) Hippocampal subfield segmentation with underlay of axial T2-weighted data c) Multi-spectral amygdala subnuclei segmentation (lateral, basal, accessory basal, central, cortical, medial nuclei and corticoamygdaloid transition area (CATA) with underlay of axial T1-weighted data d) Amygdala subnuclei segmentation with underlay of axial T2-weighted data.

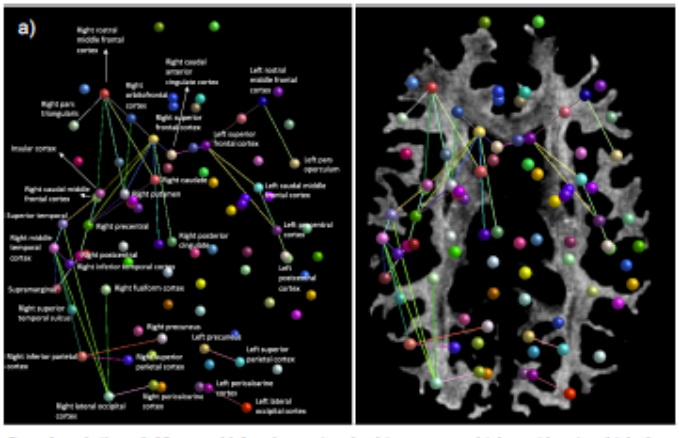

Case description: A 38-year-old female was involved in a motor vehicle accident in which she was a pedestrian hit by a car. Head CT revealed subcutaneous soft tissue swelling over the right parietal bone. Ventricles and sulci appeared normal in size and configuration and there was no midline shift or other mass effect, and grey-white matter differentiation was maintained throughout the brain. The patient received surgical staples to close a laceration over the right parietal bone. The patient reported minimal headaches or nausea, but dizziness, daytime fatigue, hypersomnolence, reduced problem-solving skills and slowed cognitive processing persisted for several weeks following the injury. Full recovery, defined as full symptom resolution and return to baseline function, was achieved approximately 6 months post-injury.

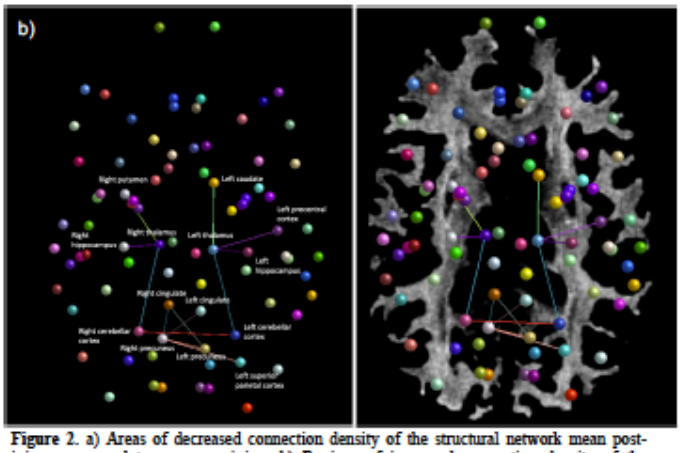

Figure 2. a) Areas of decreased connection density of the structural network mean post-injury compared to mean pre-injury b) Regions of increased connection density of the structural network mean post-injury compared to mean-pre-injury.

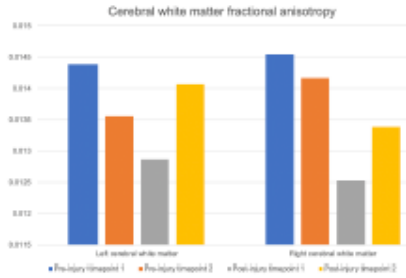

Figure 3. Fractional anisotropy of the hemispheric cerebral white matter across scanning timepoints.

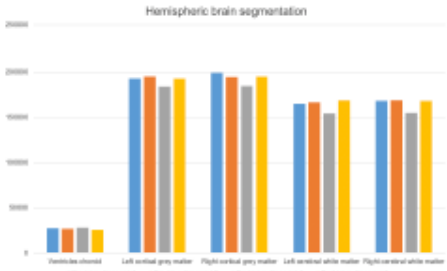

Figure 4. Volumes of choroid ventricles, hemispheric grey matter and hemispheric white matter across scanning timepoints.

The subcortical segmentation of the amygdala nuclei and hippocampal subfields did not reveal any clear changes between the scanning timepoints. At post-injury timepoint 1, the right and left hemispheric brain segmentation revealed lower cortical grey matter and cerebral white matter volume compared to other scanning timepoints (Fig. 4). Diffusion MRI connectomes pre-injury and post-injury revealed a widespread decrease in connectivity after the patient's head trauma, mainly involving connections between cortical regions (Fig. 4a). To a lesser degree, mean pre- to post-injury comparison also revealed some increased connectivity, primarily in subcortical areas and the forebrain (Fig. 2). At post-injury timepoint 1, connection density was extensively reduced, but this decrease in connectivity was partially reduced by post-injury timepoint 2. FA of the cerebral white matter was markedly reduced in both hemispheres in the first scan following the head trauma. In both the left and right hemispheres, the final timepoint scan revealed a subsequent increase of FA to levels similar to those pre-injury (Fig. 3).

Conclusion

This 7 Tesla case report demonstrates novel evidence of widespread connectivity and microstructural changes at a highly granular level after mTBI, where conventional neuroimaging at a clinical level showed no radiological abnormalities. Moreover, we suggest that diffusion-weighted investigation of TBI symptomology may be of significant use in clinical practice.

This work was funded by DOD-IDA W81XWH-19-1-0616 and NIH R01 MH109544